

11-6-2017

28-GHz Channel Measurements and Modeling for Suburban Environments

Yaguang Zhang
Purdue University, ygzhang@purdue.edu

David J. Love
Purdue University, djlove@purdue.edu

Nicolo Michelusi
Purdue University, michelus@purdue.edu

James V. Krogmeier
Purdue University, jvk@purdue.edu

Christopher R. Anderson
United States Naval Academy, canderso@usna.edu

See next page for additional authors

Follow this and additional works at: <http://docs.lib.purdue.edu/ecetr>

Zhang, Yaguang; Love, David J.; Michelusi, Nicolo; Krogmeier, James V.; Anderson, Christopher R.; Jyoti, Soumya; and Sprintson, Alex, "28-GHz Channel Measurements and Modeling for Suburban Environments" (2017). *Department of Electrical and Computer Engineering Technical Reports*. Paper 483.
<http://docs.lib.purdue.edu/ecetr/483>

Authors

Yaguang Zhang, David J. Love, Nicolo Michelusi, James V. Krogmeier, Christopher R. Anderson, Soumya Jyoti, and Alex Sprintson

28-GHz Channel Measurements and Modeling for Suburban Environments

Yaguang Zhang, Soumya Jyoti, Christopher R. Anderson,
David J. Love, Nicolo Michelusi, Alex Sprintson, and James V. Krogmeier

Abstract—This paper presents millimeter wave propagation measurements at 28 GHz for a typical suburban environment using a 400-megachip-per-second custom-designed broadband sliding correlator channel sounder and highly directional 22-dBi (15° half-power beamwidth) horn antennas. With a 23-dBm transmitter installed at a height of 27 m to emulate a microcell deployment, the receiver obtained more than 5000 power delay profiles over distances from 80 m to 1000 m at 50 individual sites and on two pedestrian paths. The resulting basic transmission losses were compared with predictions of the over-rooftop model in recommendation ITU-R P.1411-9. Our analysis reveals that the traditional channel modeling approach may be insufficient to deal with the varying site-specific propagations of millimeter waves in suburban environments. For line-of-sight measurements, the path loss exponents obtained for the close-in (CI) free space reference distance model and the alpha-beta-gamma (ABG) model are 2.00 and 2.81, respectively, which are close to the recommended site-general value of 2.29. The root mean square errors (RMSEs) for these two reference models are 9.93 dB and 9.70 dB, respectively, which are slightly lower than that for the ITU site-general model (10.34 dB). For non-line-of-sight measurements, both reference models, with the resulting path loss exponents of 2.50 for the CI model and 1.12 for the ABG model, outperformed the site-specific ITU model by around 14 dB RMSE.

Index Terms—Millimeter wave, channel measurements, channel modeling, suburban environments

I. INTRODUCTION

The increasing demand of mobile device users for higher data rates has been the driving factor for the rapid development of mobile telecommunications during the past decade [1]. The number of worldwide mobile subscriptions, which reached a record height of 7.5 billion in 2016, has continued to increase, and the total mobile data traffic is expected to rise at a compound annual growth rate of 42% between the end of 2016 and 2022 [2]. This increasing usage of wireless technology is prompting mobile service providers to take advantage of higher frequency bands in the foreseeable future, starting with millimeter waves (mm-waves), to overcome the expected global bandwidth shortage [3].

Y. Zhang, D. J. Love, N. Michelusi, and J. V. Krogmeier are with the School of Electrical and Computer Engineering, Purdue University, 465 Northwestern Avenue, West Lafayette, IN 47907, USA. (Email: {ygzhang, djlove, michelus, jvk}@purdue.edu)

C. R. Anderson is with the Department of Electrical and Computer Engineering, United States Naval Academy, 105 Maryland Ave, Annapolis, MD 21402, USA. (Email: canderso@usna.edu)

S. Jyoti and A. Sprintson are with the Department of Electrical and Computer Engineering, Texas A&M University, College Station, TX 77843, USA. (Email: {soumyajyoti.jh, spalex}@tamu.edu)

Sponsorship for this work was provided by NSF research grant 1642982.

With recent advances in radio frequency (RF) technology [4]–[6], hardware operating at mm-wave frequencies is becoming commercially available [7]–[9]. This has made mm-wave frequencies the most promising higher frequency bands for a larger usable radio spectrum. To fully understand the propagation characteristics of mm-wave signals, the amount of research on mm-wave channel measurement and modeling has increased dramatically in the past five years [1], [10]–[12]. However, the majority of current research on mm-wave communications has focused on urban areas with high population densities, with very few measurement campaigns for suburban and rural environments, which are also important for future mobile networking technologies. Moreover, point-to-point links have received significant attention, but the channel information provided by this approach is insufficient for next-generation wireless networks such as 5G. These networks must address mobility requirements because frequent and location-specific blockages are expected for mm-waves, which require a much richer set of channel state information beyond LoS path loss (such as multipath scattering).

In this paper, we explore this gap in the research by focusing on suburban environments and constructing physically-motivated and practical models that can be used for mm-wave networks in these environments. An intensive measurement campaign has been carried out at the United States Naval Academy (USNA) in Annapolis, Maryland. Measurements were taken around the campus at 28 GHz to characterize the propagation in a suburban-type environment. The resulting path losses are compared with several standard 5G channel models. Our results indicate that a holistic, network-wide approach beyond traditional point-to-point links may be needed to deal with the high dependence of mm-waves on site-specific environment geometry.

The paper is organized as follows: In Section II, we present our propagation measurements in suburban environments; In Section III, we present the procedure for calculating basic transmission losses, followed by our analysis in Section IV; Finally, in Section V, we conclude the paper.

II. MM-WAVE PROPAGATION MEASUREMENTS FOR SUBURBAN ENVIRONMENTS

An outdoor propagation measurement campaign was conducted on the USNA campus to emulate a typical 5G deployment in a suburban environment. The transmitter (TX) was temporarily installed on the Mahan Hall clock tower. The

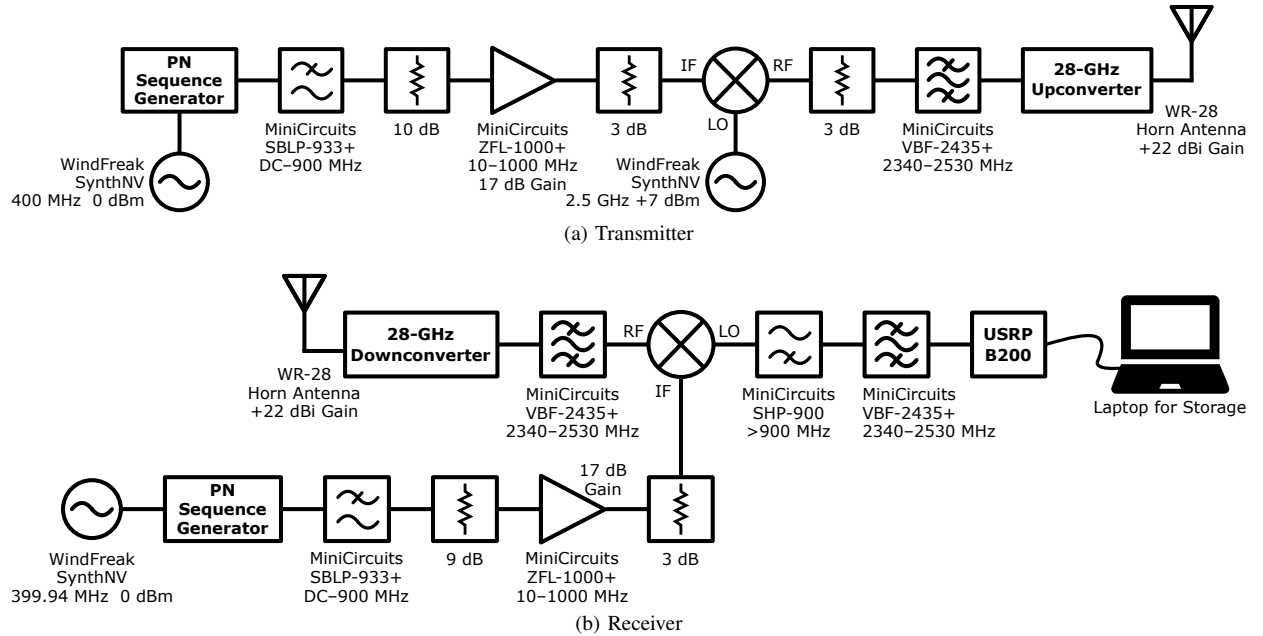


Fig. 1. Block diagrams for the 28-GHz broadband sliding correlator channel sounder. Model numbers are labeled for some commercially available parts.

receiver (RX) was moved around the campus to obtain path loss measurements for individual sites and continuous paths.

A. Measurement Equipment

A custom-designed broadband sliding correlator channel sounder [13] was used to record propagation data. Figure 1 presents block diagrams for the channel sounder. At both the TX and the RX sides, horn antennas with a nominal +22 dBi gain and 15° half-power beamwidth (HPBW) were employed, and pseudo-random noise (PN) generators produced the same PN sequences with a chip sequence length of 2047 [1].

At the TX, the PN probing signal was generated with a chip rate of 400 megachips per second (Mcps). It was first modulated to a 2.5-GHz intermediate frequency (IF) and then converted to RF of 28 GHz by mixing it with a 25.5-GHz local oscillator (LO) at the upconverter. At the RX, the received signal was first downconverted from 28 GHz to 2.5 GHz and then cross-correlated with the identical PN sequence generated with a slightly slower clock rate of 399.94 MHz, similar to the setup in [1]. A Universal Software Radio Peripheral (USRP) B200 was utilized to record the resulting in-phase (*I*) and quadrature (*Q*) signal components. It also regularly sampled the RX's location with the help of an on-board GPS disciplined oscillator (TCXO version). The implementation of the measurement system is shown in Figure 2.

Table I summarizes the key parameters for the channel sounder. Note that the estimation for the maximum measurable path loss is based on the following. (1) The RX low-noise amplifier has a noise figure of 2.4 dB, so we assume a worst-case RX noise figure of 6 dB. (2) The RX detection bandwidth is 60 kHz. (3) The estimated minimum signal-to-noise ratio (SNR) for a detectable signal is 5 dB.

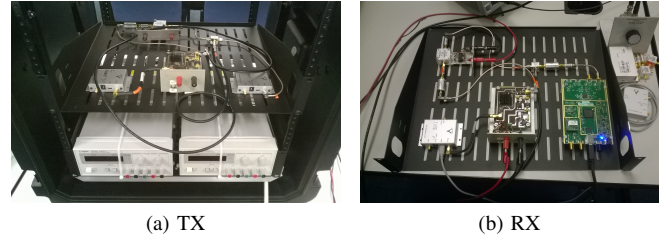


Fig. 2. Photos of the custom-designed spread-spectrum channel sounder. Components are fixed on shelves for portability and the TX is further more enclosed into a rack case for extra protection during the deployment.

TABLE I
BROADBAND SLIDING CORRELATOR CHANNEL SOUNDER
SPECIFICATIONS

Carrier Frequency	28 GHz
Chip Sequence Length	2047
RF Bandwidth (First Null)	800 MHz
TX Chip Rate	400 Mcps
Temporal Resolution	2.5 ns
RX Chip Rate	399.94 Mcps
TX Power	23 dBm
TX/RX Antenna Gain	22 dBi
Measured TX/RX Azimuth HPBW	10.1°
Measured TX/RX Elevation HPBW	11.5°
Maximum Measurable Path Loss	182 dB

B. Measurement Setup and Procedure

Three types of measurements have been performed for large-scale path loss, emulated single-input and multiple-



(a) RX on an Electric Car



(b) RX on a Trolley



(c) Before a Continuous Signal Recording for a Pedestrian Path

Fig. 3. Photos of the measurement setup. The TX was installed on a clock tower at a height of 90 feet (27.4 m) to emulate a microcell deployment. Either an electric car or a two-layer trolley was used to transport the RX. For both cases, the platform for the RX could be rotated horizontally and tilted with composite wood shims to align the beam.

output (SIMO), and continuous tracks. The TX was installed at a height of 90 feet (27.4 m) to emulate a microcell deployment. The RX was moved around campus by an electric car or a two-layer platform trolley to obtain the measurements, which is illustrated by the photographs in Figure 3.

We used compasses and digital levels to achieve beam alignment prior to the measurements at each RX location. Aside from the USRP output files and GPS samples, the azimuths and elevations of both the TX and RX antennas were recorded manually. This allowed us to reconstruct the geometry relationship of the antennas and extract precise antenna gains. The USRP gain was manually adjusted to maximize the SNR at the RX.¹

1) Large-Scale Path Loss Measurements: Forty measurement locations were chosen to investigate the large-scale path loss at various distances from the TX (between 100 m and 1000 m). For each site, the RX antenna was moved along X and Z axes by our positioning system to form a “+” pattern within a $20\lambda \times 20\lambda$ area, where $\lambda = 10.7$ mm was the wave length corresponding to 28 GHz. For every λ interval on the “+” pattern, one 3-second signal recording and one GPS sampling were obtained, with 40 separate measurements in total. In Figures 3b and 3c, the custom-built X-Z positioning system is shown.

¹The Python code for automatically carrying out the measurements at each location using GNU Radio, together with the MATLAB code for post-processing the collected data, are available at <https://github.com/YaguangZhang/EarsMeasurementCampaignCode.git>

2) Emulated SIMO Measurements: Measurements that were used to emulate SIMO signals were similar to those for the large-scale path loss, but with a higher space sample density and a larger sample area for each site. The RX antenna was moved along the “+” pattern with the interval between adjacent measurements reduced to 0.25λ . The pattern covered an enlarged $40\lambda \times 40\lambda$ area, with 320 separate measurements in total for each site. Ten locations were chosen, and the TX and RX distances varied from 50 m to 500 m. The data collected were or will be used to analyze small-scale propagation characteristics. However, in this paper, we focus only on the large-scale path loss.

3) Measurements for Continuous Tracks: To investigate the shadowing effect on a moving user, two approximately 200-m-long straight tracks were chosen for continuous signal recordings. The RX antenna was fixed on the positioning system and moved at walking speed along each track to record the signal, and the GPS location of the RX was sampled once per second. The RX antenna elevation was kept at 0° , and the platform was adjusted as necessary to maintain the azimuth with respect to the fixed earth reference during the recording process (see Figure 3c).

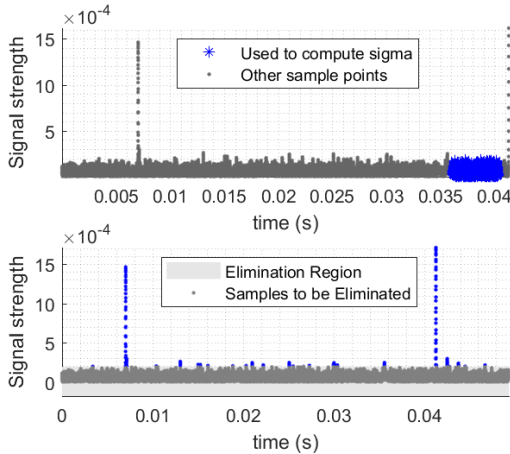
III. BASIC TRANSMISSION LOSS CALCULATION

In this section, we present our procedure for computing the basic transmission loss of each signal recording. Received signal power calculation, RX calibration, antenna pattern generation, and antenna gain extraction were considered in determining antenna-independent path losses.

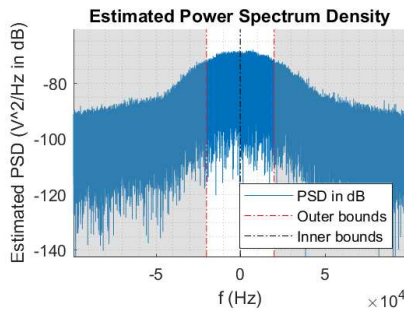
A. Received Signal Power Calculation

The traditional method of calculating received signal power for broadband measurements is carried out in the time domain by integrating the total area under a power delay profile (PDP), assuming that all the multipath signals add up in phase. Instead, we adopted a frequency-domain technique, the process of which is summarized below, to preserve the phase relationships and yield a more accurate estimate of received power.

- 1) Run the recorded complex I/Q voltage waveform through a 60 kHz low pass filter (LPF) to remove noise in frequency.
- 2) Further eliminate noise in the time domain by (a) estimating the standard deviation σ and mean n_0 for the noise using 10%–20% of the samples between two adjacent signal pulses, as illustrated in the top plot of Figure 4a; (b) calculating the noise elimination threshold as $3.5\sigma + n_0$; and (c) Setting all samples with an amplitude below the threshold to 0, as illustrated by the plot at the bottom of Figure 4a.
- 3) Calculate the received power by integrating over the power spectrum density (PSD) of the noise-eliminated signal. We chose a tighter integration range (1 Hz–20 kHz) to ignore residual high-frequency noise and direct current (DC) components, as illustrated in Figure 4b.



(a) Noise Variance Estimation and Noise Elimination



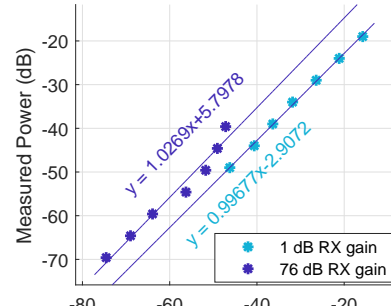
(b) Integral in Frequency for Signal Power

Fig. 4. Received signal power calculation. (a) For each measurement, the noise amplitude characteristics were first estimated for the filtered signal to set a noise elimination threshold. Then, all samples weaker than the threshold were set to 0. (b) The received power energy was computed by integrating the PSD of the noise-eliminated signal below 20 kHz, ignoring the DC component.

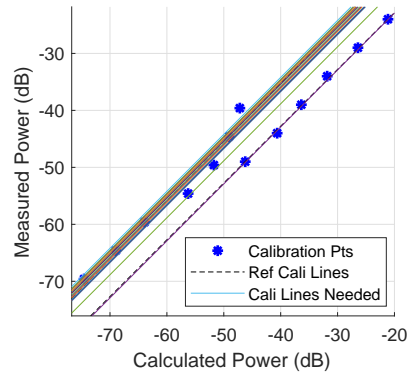
The resulting values would have a linear relationship with the actual received power. Next, we needed the RX calibration to convert the calculated power to the received power.

B. RX Calibration

To calibrate the RX, the upconverter and downconverter, as well as the antennas, were removed from our system in Figure 1. Then, an adjustable attenuator for IF signals with a 5-dB step size was attached to the TX to simulate the channel. The RX together with a spectrum analyzer were used to record and measure the signal strength separately for a set of different attenuation values, with the results from the spectrum analyzer treated as the reference for signal strengths. We repeated the procedure with the RX gain (i.e., the adjustable USRP gain) set as its minimum (1 dB) and maximum (76 dB) values. From the obtained power value pairs, linear relationships were extracted for expected measured power vs. calculated power at the RX gain limits [14]. Figure 5 shows the resulting two base reference calibration lines obtained via orthogonal least squares, as well as all the calibration lines needed for our whole dataset gotten via a linear interpolation over the



(a) Base Calibration Lines



(b) Linearly Interpolated Calibration Lines

Fig. 5. Linear fitting and interpolation for RX calibration lines. (a) By carrying out orthogonal least squares over the calibration data points, a linear relationship was constructed between the calculated power and the reference power measured by the spectrum analyzer. (b) Calibration lines needed for the whole dataset were obtained via a linear interpolation over the RX gain with fixed unit slopes.

RX gain. With these results, received powers were computed accordingly.

C. Antenna Pattern Generation

Using calibrated measurements from the manufacturer as a reference, we were able to account for upconverter/downconverter and antenna gains.

1) *Normalization for Antenna Plane Patterns:* To construct the pattern for our antennas, two measurement sweeps were conducted in an anechoic chamber at USNA for the azimuth and elevation planes, respectively, using an Anritsu VectorStar MS4640 series Vector Network Analyzer and the Diamond Engineering DAMS Antenna Measurement System. The forward transmission coefficients $|S21|$ from each sweep were normalized to the nominal maximum gain of the antennas at 28 GHz, +22 dBi, and the resulting antenna patterns are plotted in Figure 6.

2) *Full 3D Antenna Pattern Filling:* From the azimuth and elevation antenna patterns, we constructed a full 3D pattern for the antenna via linear interpolation, as illustrated in Figure 7.

3) *Antenna Gain Computation:* With the detailed measurement records collected, we were able to reconstruct the geom-

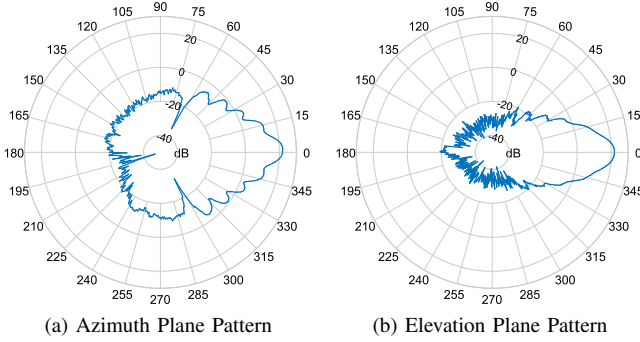


Fig. 6. Antenna pattern measurement results for the azimuth and elevation planes. The antenna beamwidths (10.1° azimuth HPBW and 11.5° elevation HPBW) were computed accordingly.

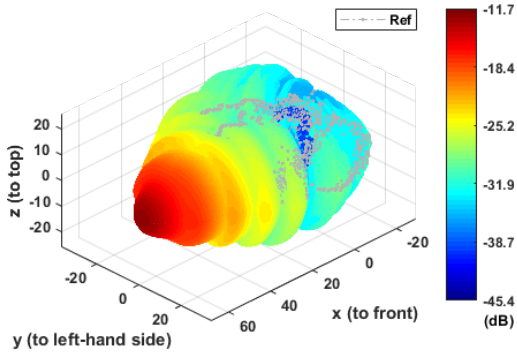


Fig. 7. Full 3D antenna pattern filling.

etry relationship of the TX and RX antennas for each measurement and extract their gains. Figure 8 gives an illustration for computing the TX antenna gain for one measurement. As we can see, the Universal Transverse Mercator (UTM) coordinate system (x, y) was extended with altitude z to form a three-dimensional (3D) reference system (x, y, z). Inside, a new 3D coordinate system (X, Y, Z) was constructed originating at the antenna of interest, which could be for either the TX or the RX, so that the azimuth and elevation for any destination point could be calculated. The corresponding gain was extracted by interpolating the antenna measurement data in 3D.

IV. MEASUREMENT RESULTS AND ANALYSIS

In Figure 9, 49 of the 50 static sites are shown on a Google map of the USNA campus. One large-scale site was ignored in our analysis because the data collected there were influenced by rain.

A. Line-of-Sight (LoS) Sites

For LOS sites (24 in total), we compared the measurement results with the International Telecommunication Union (ITU) site-general model for propagation over rooftops [15]:

$$PL(d, f) = 10 \cdot \alpha \cdot \log_{10}(d) + \beta + 10 \cdot \gamma \cdot \log_{10}(f) + N(0, \sigma), \quad (1)$$

where d is the 3D direct distance between the TX and RX in meters and f is the operating frequency in GHz. In our case,

$f = 28$ GHz. The parameters α , β , γ , and σ are chosen for the LoS propagation in a suburban environment [15]:

$$\left\{ \begin{array}{l} \alpha = 2.29 \\ \beta = 28.6 \\ \gamma = 1.96 \\ \sigma = 3.48 \end{array} \right. \quad (2)$$

These parameters are recommended for a distance range 55 m to 1200 m at 2.2–73 GHz frequency.

For a better comparison, we also considered two other models. The first is the close-in (CI) free space reference distance path loss model:

$$PL(d) = PL_{FS}(d_0) + 10 \cdot n \cdot \log_{10}\left(\frac{d}{d_0}\right), \quad (3)$$

$$PL_{FS}(d_0) = 20 \cdot \log_{10}\left(\frac{4\pi d_0}{\lambda}\right), \quad (4)$$

where n is the path loss exponent, $PL_{FS}(d_0)$ is the free-space propagation loss at a distance of $d_0 = 1$ m with isotropic antennas, and λ is the carrier wavelength. The second is the alpha-beta-gamma (ABG) model on which the ITU site-general model is based:

$$PL(d) = 10 \cdot \alpha \cdot \log_{10}(d) + \beta + 10 \cdot \gamma \cdot \log_{10}(f). \quad (5)$$

Note that α here acts as the path loss exponent.

We have fit these two reference models to our LoS measurement results. To deal with GPS sample errors, the median values of latitude, longitude, and altitude measurements for each site were used as that site's geographic location to compute the site distance to the TX. And for the ABG model, we set $\gamma = 1.96$ as recommended by ITU, given that we had only one carrier frequency at 28 GHz.

All three models, together with the measurement results, are presented in Figure 10a. The ITU model provides path loss predictions in the form of Gaussian variables, and their 3-sigma range covers the measured path losses reasonably well, even though if we extrapolate the ITU model to $d = d_0 = 1$ m, its mean path loss would be smaller than the corresponding free-space propagation loss (FSPL). This issue affects the ABG type of models in general. In our case, the ABG model has the lowest root mean square error (RMSE) at 9.70 dB, but its predicted path loss quickly descends below FSPL as the distance decreases. Hence, the ABG model does not generalize well outside the distance range for its measurement data.

The resulting path loss exponents for the CI and ABG reference models are 2.00 and 2.81, respectively. For the LoS dataset, these two models perform 0.41 dB and 0.64 dB better than the ITU model, respectively, in terms of RMSE. Basically, within the distance range of the LoS measurement dataset, these three models are equivalent, and the ITU model performs well..

The four sites with lower path loss than the ITU 3-sigma range were further investigated through their PDPs. As very strong multipath components showed up for all of these sites, it is still possible for even narrow mm-waves to have

multipath components that dramatically enhance the signal. For the closer two sites, this was expected because they were surrounded by buildings. However, the two sites at farther distances were in open areas, and the most reasonable origins of the multipath would be reflections from buildings close to the TX as many of these buildings have sloped ceilings.

B. Non-Line-of-Sight (NLoS) Sites

For the 25 NLoS sites, the site-specific model for propagation over rooftops defined in ITU-R P.1411-9, Section 4.2.2.2 [15] was utilized to predict the path loss for each site. Similar to the LoS case, the CI and ABG models were

compared with the ITU model as references. This time, γ was set to 2.30 for the ABG model, as recommended by ITU for NLoS above-rooftop propagation from 260 m to 1200 m at 2.2–66.5 GHz in an urban high-rise environment, which was the most suitable for our purposes.

Figure 10b shows the ITU predictions together with the reference models and NLoS measurement results. For the NLoS data, the ITU model shows a trend of following the measured path loss, but it has over-estimated predictions for most of the sites. Only five of the NLoS sites had measured path losses that were clearly larger than the corresponding

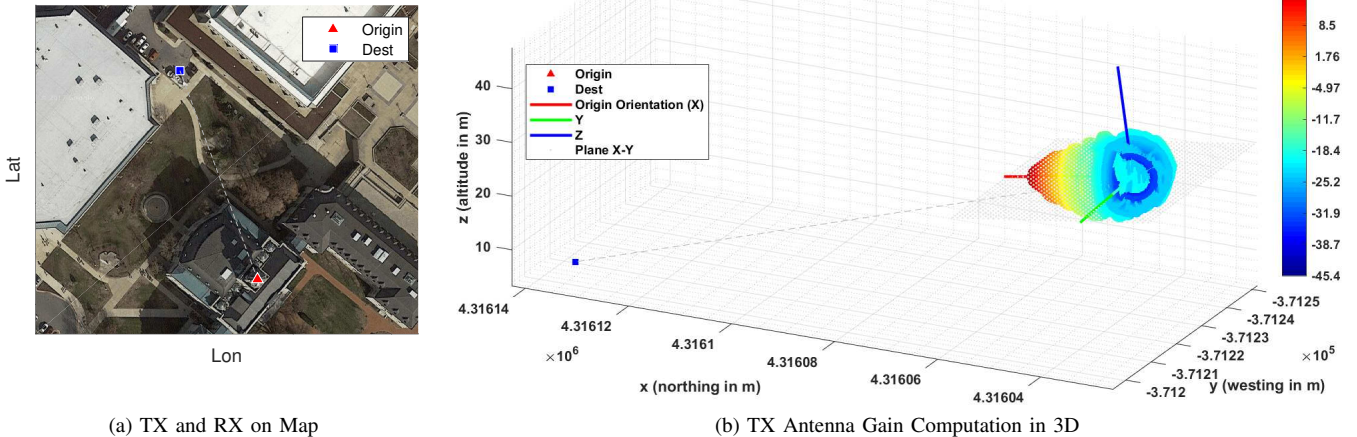


Fig. 8. Illustration for antenna gain computation. First, within an extended UTM coordinate system, the azimuth and elevation for the destination, from the origin's point of view, were calculated. Then, the resulting gain for the antenna located at the origin were extracted via 3D antenna pattern interpolation. For the case illustrated, the antenna of interest was the TX on the clock tower. From its point of view, i.e. in the tilted coordinate system (X, Y, Z) which was determined by the TX antenna's orientation, the destination has an azimuth of 15.2° and an elevation of -3.9° . The corresponding gain by the 3D interpolated antenna pattern was 11.05 dB.

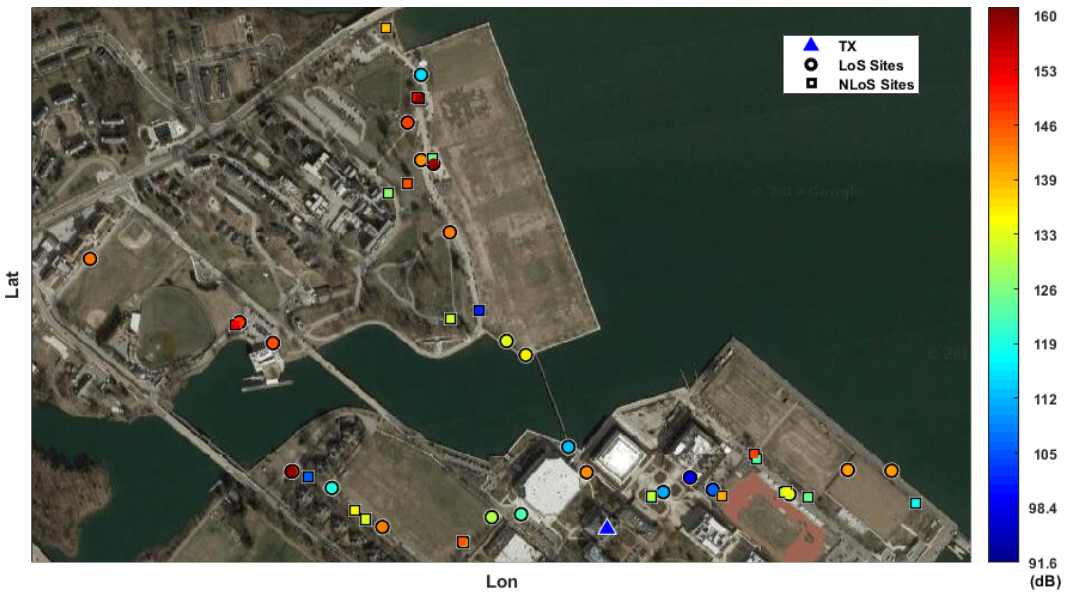


Fig. 9. Overview for the basic transmission losses of the large-scale and SIMO measurements. The geographic locations for the measurement sites are shown on a Google map of the USNA campus, with their corresponding worst-case basic transmission losses illustrated by color labels.

TABLE II
KEY PARAMETERS FOR CHANNEL MODELS

Model	LoS					NLoS				
	n	α	β	γ	RMSE (dB)	n	α	β	γ	RMSE (dB)
ITU	N/A	2.29	28.6	1.96	10.34	N/A	N/A	N/A	N/A	25.33
Close-in	2.00	N/A	N/A	N/A	9.93	2.50	N/A	N/A	N/A	11.73
ABG	N/A	2.81	11.66	1.96	9.70	N/A	1.12	63.61	2.30	11.05

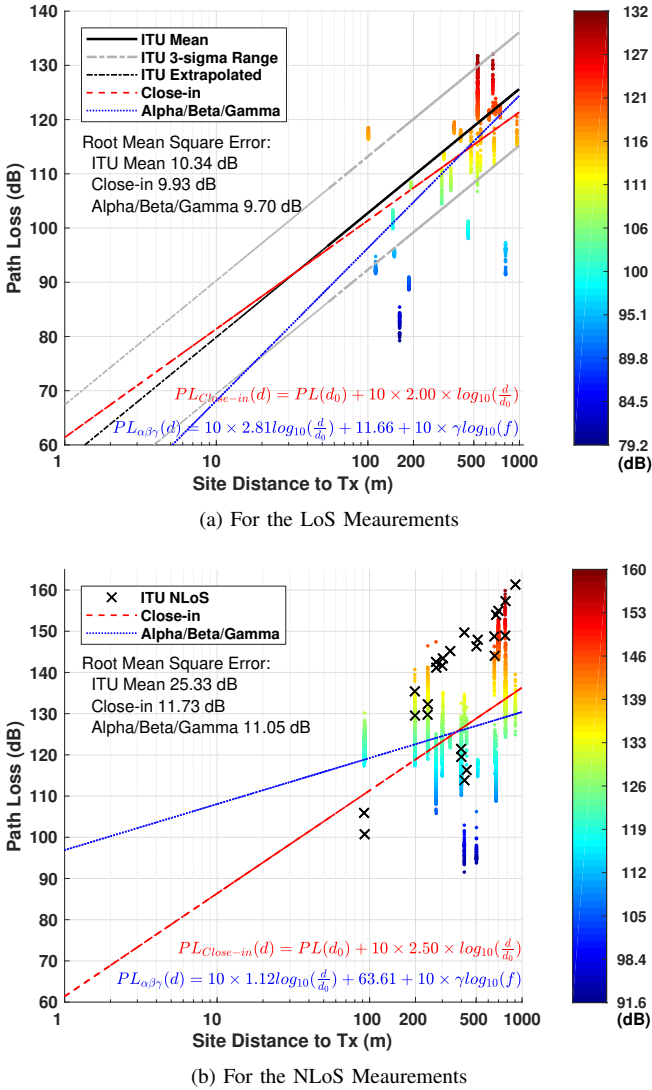


Fig. 10. Model comparison for LoS and NLoS measurements. (a) In the LoS case, the ITU predictions agree reasonably well with our measurement results, as well with the reference models. (b) For NLoS sites, the ITU predictions show a trend of following the measurement results but overestimate the path loss for most of these sites.

ITU predictions. Furthermore, the ABG model does not agree well with the close-in one, with resulting path loss exponents of 1.37 and 2.50, respectively. This may be caused by an over-fitting of the ABG model to our NLoS path losses. However, both of these reference models outperformed the ITU predictions by around 14 dB RMSE. Table II summarizes

the key parameters for the obtained channel models.

Several factors may have reduced the performance of the ITU site-specific model. First, the buildings on the USNA campus are not geometrically arranged exactly like those defined in the ITU suburban area propagation model. The over-rooftop propagations often span multiple building rows, which alters the blockage and reflection conditions. Also, for many of our sites, the ITU over-rooftop model with a limited number of buildings would be a better fit, which may ameliorate the path loss overestimation for propagations beyond the building area.

Second, the geometry defined in the ITU model does not always agree with that for our NLoS sites. For example, the street width for most of our sites was over the defined limit. For these cases, we used the upper bound for the model 25 m in the calculation, so the model may have underestimated the path losses for sites relatively close to the TX by considering reflections from buildings that do not exist. For sites that were further away, more buildings are positioned between the TX and the RX, which may have caused an overestimation.

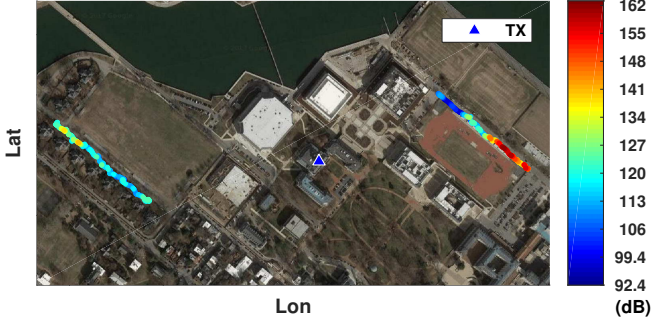
Third, at around 10 of the NLoS sites, the LoS propagation was directly blocked by vegetation, not buildings. A few other sites have foliage near their LoS paths. ITU-R P.1411-9 does not consider the propagation effects caused by vegetation due to the complexity.

C. Continuous Tracks

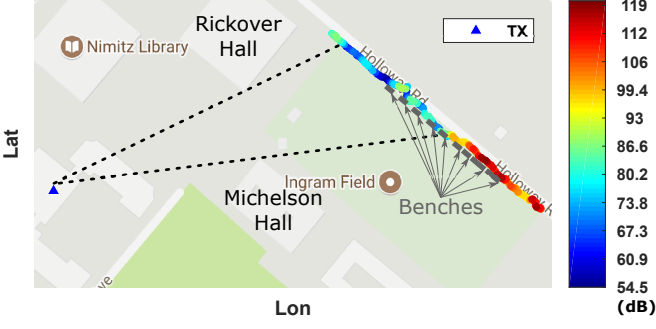
Two continuous signal recordings were conducted to investigate the shadowing effect for a simulated moving RX at walking speed. The basic transmission losses were calculated for each second of signal recording (see Figure 11).

For the track on Holloway road (Figure 11b), the most significant blockage was from Michelson Hall, which caused approximately 30 dB of additional path loss to half of the track. Rickover Hall partially blocked the track by around 20 dB. The dotted lines in Figure 11b show where these blockages started on the track. There were also metal stadium benches on the northeast side of Ingram Field adjacent to the measurement route, which caused around 20 dB of additional path loss. This is more clear on the part of the track with no building blockages, where a path loss peak shows up behind each one of the benches.

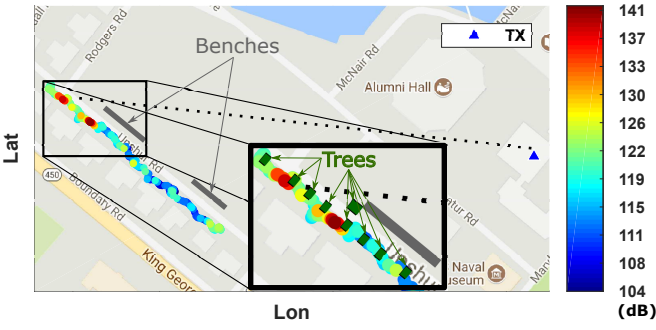
For the track on Upshur road (Figure 11c), the two benches next to the measurement route were farther away from the track and did not block the signal significantly. For this set of data, the effect of foliage shadowing is of interest. Trees were



(a) Basic Transmission Losses for Continuous Tracks Shown on a Google Map of the USNA Campus



(b) Track on Holloway Road



(c) Track on Upshur Road

Fig. 11. Basic transmission losses for continuous tracks. The path losses on Holloway road illustrate the shadowing effect of buildings and benches, while those on Upshur road illustrate the shadowing effect of trees. In (c), the starting part of the track is zoomed in, and trees are indicated by green rectangles.

planted on the TX side adjacent to the pathway, and a few path loss peaks shown on Figure 11c correspond well with the locations of these trees.

D. Discussion

We have focused on large-scale path loss, comparing our measurements with predictions obtained by following ITU-R P.1411-9 [15] on propagation over rooftops. Our data shows that a richer set of channel state information, including multipath scattering and location-specific building geometries, are necessary to produce more reliable coverage predictions. In the LoS situation, the measurements agree reasonably well with the ITU predictions, while for the NLoS situation, most of the predictions appear to be higher than the corresponding

measurement results. Limiting the building number, extending the model with sloped ceilings, and considering over-rooftop propagations spanning multiple building rows may help improve the ITU site-specific model for suburban environments.

According to our model comparison results, the CI and ABG models do a good job of predicting large-scale path loss in both LoS and NLoS cases. Furthermore, the ABG model, in general, is able to provide a better fit for a given set of data. However, it may give non-physical results beyond the distance range over which the data are collected. Because of this, care should be taken when using the ABG model out of its defined range.

The continuous recordings back up channel modeling attempts that consider environmental information, for example, through the radio environment map [16] and ray tracing [17] approaches. Moreover, the results indicate the possibility of increasing large-scale path loss prediction accuracy for statistical models with simple but site-specific environment geometry, which would balance computation complexity and model performance.

E. Future Works

In the future, we plan to: (1) Further investigate the ITU channel modeling recommendation for possible extensions or improvements, e.g. sloped ceilings, over roof-tops propagations spanning multiple rows, and limitation on the building number; (2) Explore the possibility of enhancing statistical channel model performance with side geometric information; (3) Examine the influence on large-scale path loss from the vegetation; (4) Look closer into the SIMO measurements for means to utilize the presented multipath effects.

V. CONCLUSION

In this paper, we discussed the implementation of a custom-designed broadband channel sounder and explained how we used it for a measurement campaign that focused on the propagation of mm-waves in suburban environments at 28 GHz. The resulting basic transmission losses for LoS and NLoS sites were separately compared with the corresponding propagation predictions based on the ITU-R P.1411-9 recommendation. The site-general LoS model for propagation over rooftops in suburban environments agreed with our measurements reasonably well, but the corresponding site-specific NLoS model overestimated the path loss for most of the NLoS sites. Two continuous measurement tracks were also constructed. The results illustrated that a knowledge of geometric features may increase the prediction performance for large-scale path losses, which backs up the radio environment map approach for channel modeling in future communication networks.

ACKNOWLEDGMENT

We would like to thank the faculty members from the Department of Electrical and Computer Engineering at the United States Naval Academy for their kind assistance during the measurement campaign.

REFERENCES

- [1] T. S. Rappaport *et al.*, "Millimeter wave mobile communications for 5g cellular: It will work!" *IEEE access*, vol. 1, pp. 335–349, 2013.
- [2] "Ericsson mobility report june 2017," Ericsson, SE-164 80 Stockholm, Sweden, Tech. Rep., June 2017. [Online]. Available: <https://www.ericsson.com/assets/local/mobility-report/documents/2017/ericsson-mobility-report-june-2017.pdf>
- [3] T. S. Rappaport, R. W. Heath Jr, R. C. Daniels, and J. N. Murdock, *Millimeter Wave Wireless Communications*. Pearson Education, 2014.
- [4] K. Okada *et al.*, "Full four-channel 6.3-gb/s 60-ghz cmos transceiver with low-power analog and digital baseband circuitry," *IEEE Journal of Solid-State Circuits*, vol. 48, no. 1, pp. 46–65, 2013.
- [5] N. Saito *et al.*, "A fully integrated 60-ghz cmos transceiver chipset based on wigig/ieee 802.11 ad with built-in self calibration for mobile usage," *IEEE Journal of Solid-State Circuits*, vol. 48, no. 12, pp. 3146–3159, 2013.
- [6] D. Fritzsche, G. Tretter, C. Carta, and F. Ellinger, "Millimeter-wave low-noise amplifier design in 28-nm low-power digital cmos," *IEEE Transactions on Microwave Theory and Techniques*, vol. 63, no. 6, pp. 1910–1922, 2015.
- [7] Z. Pi and F. Khan, "An introduction to millimeter-wave mobile broadband systems," *IEEE Communications Magazine*, vol. 49, no. 6, 2011.
- [8] S. Rangan, T. S. Rappaport, and E. Erkip, "Millimeter-wave cellular wireless networks: Potentials and challenges," *Proceedings of the IEEE*, vol. 102, no. 3, pp. 366–385, 2014.
- [9] W. Roh *et al.*, "Millimeter-wave beamforming as an enabling technology for 5g cellular communications: Theoretical feasibility and prototype results," *IEEE Communications Magazine*, vol. 52, no. 2, pp. 106–113, 2014.
- [10] G. R. MacCartney and T. S. Rappaport, "73 ghz millimeter wave propagation measurements for outdoor urban mobile and backhaul communications in new york city," in *IEEE International Conference on Communications (ICC), 2014*. IEEE, 2014, pp. 4862–4867.
- [11] A. I. Sulyman, A. T. Nassar, M. K. Samimi, G. R. MacCartney, T. S. Rappaport, and A. Alsanie, "Radio propagation path loss models for 5g cellular networks in the 28 ghz and 38 ghz millimeter-wave bands," *IEEE Communications Magazine*, vol. 52, no. 9, pp. 78–86, 2014.
- [12] S. Deng, M. K. Samimi, and T. S. Rappaport, "28 ghz and 73 ghz millimeter-wave indoor propagation measurements and path loss models," in *IEEE International Conference on Communication Workshop (ICCW), 2015*. IEEE, 2015, pp. 1244–1250.
- [13] T. S. Rappaport *et al.*, *Wireless Communications: Principles and Practice*. New Jersey: Prentice Hall PTR, 1996, vol. 2.
- [14] C. D. Rowe, "Channel propagation model for train to vehicle alert system at 5.9 ghz using dedicated short range communication," Ph.D. dissertation, Blacksburg, VA, 2016.
- [15] ITU, "Propagation data and prediction methods for the planning of short-range outdoor radiocommunication systems and radio local area networks in the frequency range 300mhz and 100ghz," Tech. Rep., June 2017. [Online]. Available: <https://www.itu.int/rec/R-REC-P.1411-9-201706-I/en>
- [16] H. B. Yilmaz, T. Tugeu, F. Alagoz, and S. Bayhan, "Radio environment map as enabler for practical cognitive radio networks," *IEEE Communications Magazine*, vol. 51, no. 12, pp. 162–169, 2013.
- [17] T. A. Thomas, H. C. Nguyen, G. R. MacCartney, and T. S. Rappaport, "3d mmwave channel model proposal," in *IEEE 80th Vehicular Technology Conference (VTC Fall), 2014*. IEEE, 2014, pp. 1–6.